frontiers | Frontiers in Astronomy and Space Sciences

TYPE Original Research
PUBLISHED 18 June 2025
DOI 10.3389/fspas.2025.1605553

OPEN ACCESS

EDITED BY
Raffaele Saladino,
University of Tuscia, Italy

REVIEWED BY
Nicola Tasinato,
Normal School of Pisa, Italy
Somnath Bhowmick,
The Cyprus Institute, Cyprus

*CORRESPONDENCE
Gerard Pareras,
gerard.pareras@uab.cat
Albert Rimola,
albert.rimola@uab.cat

RECEIVED 03 April 2025
ACCEPTED 30 May 2025
PUBLISHED 18 June 2025

CITATION
Pareras G and Rimola A (2025) Single-atom iron on silicon carbide surfaces as catalyst of Fischer-Tropsch-type reactions in astrophysical environments.
Front. Astron. Space Sci. 12:1605553.
doi: 10.3389/fspas.2025.1605553

Single-atom iron on silicon carbide surfaces as catalyst of Fischer-Tropsch-type reactions in astrophysical environments

Gerard Pareras* and Albert Rimola*

Departament de Química, Universitat Autònoma de Barcelona, Bellaterra, Spain

Silicon carbide (SiC) is a major component of interstellar dust in carbon-rich environments, but its catalytic potential in space has remained largely unexplored. In this work, we investigate how single iron atoms supported on SiC (Fe^0@SiC) can drive Fischer Tropsch-type (FTT) reactions, transforming the two most abundant gas-phase species in the interstellar medium (H_2 and CO) into more complex organic compounds, i.e., formaldehyde (H_2CO) and methanol (CH_3OH). Using density functional theory (DFT), we model the catalytic cycle on the most stable β-SiC (110) surface, revealing that H_2CO forms efficiently with relatively low activation barriers (up to 18.3 kcal mol^{-1}), while, in contrast, CH_3OH formation faces a significant energy barrier (32.6 kcal mol^{-1}) in space. Atomistic mechanistic study highlights the role of Fe^0@SiC in stabilizing reaction intermediates through Fe-H-Si bridging interactions, which facilitate H_2 activation and CO hydrogenation. Kinetic analysis suggests that H_2CO and CH_3OH formation is viable in regions with temperatures above 200 and 350 K, respectively, aligning with observations of formaldehyde and methanol in protoplanetary disks and comets. The findings also suggest that FTT processes could contribute to the formation of other organic molecules, such as acetaldehyde and short-chain hydrocarbons, in space. This work offers new insights into how cosmic dust grains might drive the formation of complex molecules during the planetary system formation.

KEYWORDS

Fischer-Tropsch, silicon carbide, density functional theory, astrochemistry, heterogeneous catalysis, surface modelling, CO activation, reaction mechanisms

1 Introduction

Solid-state dust grains are prevalent in the interstellar medium, which are believed to form in circumstellar shells, considered to be dust grain condensation zones. Dust grains, typically ranging from 0.1 to 10 μm in size, are primarily composed of refractory materials such as magnesium silicates, which can incorporate elements like iron and titanium (Lodders and Fegley, 1999; Jones, 2001). The composition of these grains depends on the carbon-to-oxygen (C/O) ratio where they form. In oxygen-rich circumstellar envelopes, where local thermodynamic equilibrium (LTE) conditions dominate, silicates constitute the most common solid phase (Marini and Tosi, 2025). Conversely, in carbon-rich environments, carbonaceous materials are prevalent, which known to the date can be silicon carbide (SiC), amorphous carbon (which can be aliphatic hydrogenated-rich and aromatic

hydrogenated-poor), graphite and polycyclic aromatic hydrocarbons (PAHs) (Herrero et al., 2022). Some of these refractory materials have been identified through mid-infrared (IR) observational measurements detecting the lattice vibrations assigned to the Si–O and Si–C stretching modes at ~9 and 11 μm, respectively. Moreover, chemical analysis of presolar grains, like meteoritic and interplanetary dust particles, also indicate the presence of these (and other) materials (Kwok, 2004). However, not all grains necessarily form under LTE conditions. Shock waves induced by stellar pulsations and mass loss can cause significant deviations from equilibrium, and the presence of refractory-type circumstellar molecules in the gas phase further supports the existence of non-LTE environments (Lodders and Amari, 2005; Gobrecht et al., 2016). SiC in particular, has also been widely detected in presolar meteorites and in cometary materials returned by the Stardust mission (Hoppe, 2009; Speck et al., 2005; Fujiyoshi et al., 2015). In carbon-rich environments, SiC grains are primarily identified through their characteristic infrared emission band at ~11 μm, which, in rare cases, appears in absorption. Comparisons of astronomical spectra with laboratory and meteorite sample data indicate the material to be the β-SiC polymorph (Clement et al., 2003; Speck et al., 1999). Despite its widespread presence in circumstellar environments, there is no clear evidence of SiC in the interstellar medium, possibly due to the oxidation of grains (Whittet et al., 1990). However, it has recently been detected in the proto-planetary disk of the pre-main-sequence object SVS-13 (Fujiyoshi et al., 2015). Notably, SiC exists in multiple crystalline polytypes, meaning the ~11 μm feature is not unique to a single structural form but rather serves as a general indicator of SiC dust grains (Brown et al., 2006).

The presence of SiC is of great interest because it can act as a catalyst for the formation of PAHs (Tielens, 2008; Zhang et al., 2015; Delaunay et al., 2015; Ridgway et al., 1976; Fonfria et al., 2008). Although the complete mechanism behind the cosmic PAH formation remains debated, (Carelli et al., 2011; Woods et al., 2002; Cole et al., 1984; Frenklach et al., 1989; Cherchneff, 2011), one possible mechanism suggest that silicates can catalyse the formation of PAHs through a Lewis acid catalytic process involving acetylene reactions (Tian et al., 2012; Tian et al., 2013; Zhao et al., 2016). Additionally, SiC has been proposed as a key player in the formation of interstellar fullerenes through shock processing of circumstellar SiC grains. Laboratory experiments indicate that shock heating of SiC grains in circumstellar gas can lead to fullerene formation, even in hydrogen-rich environments (Goel et al., 2004; Bernal et al., 2022; Chen et al., 2022; Ziurys, 2024).

From an astrochemical perspective, SiC has been postulated to act as a catalyst for the formation of carbon-bearing molecules through a top-down mechanism, (Roy et al., 2023), and can be further exploited as a support material for other reactive species. In terrestrial chemistry, SiC has gained attention due to its potential applications in high-power electronic devices, owing to its high thermal conductivity, high electrical breakdown strength, and high maximum current density (Ba et al., 2015; Church et al., 2012; Vannice et al., 1986; Bhatnagar and Baliga, 1993). While SiC is not traditionally known as a catalytic material, the large surface area and high chemical inertness of β-SiC make it an excellent catalyst support, a property that has been applied in various heterogeneous catalytic reactions. For instance, it has been reported the partial oxidation of methane over a Ni/SiC catalyst (Sun et al., 2005).

One of the persistent challenges in astrochemistry is the so-called "missing iron problem", the lack of observational evidence for iron despite its expected abundance (Psaradaki et al., 2023). The prevailing hypothesis suggests that iron is sequestered from the gas phase and incorporated into dust grains through various mechanisms, including single-atom and nanocluster deposition, as well as incorporation into mineral structures such as Fe-bearing olivines and pyroxenes, or in the form of troilite (FeS) (Kemper et al., 2002; Bradley, 1994; Altobelli et al., 2016; Ishii et al., 2018; Sargent et al., 2009; Sasaki et al., 2001). Given its structural and chemical properties, SiC is an ideal candidate for supporting iron deposition in these forms.

In this study, a SiC surface with the deposition of single Fe atoms (Fe^0@SiC) was atomistically modelled and its capacity to catalyse Fischer Tropsch-type (FTT) reactions investigated. FTT reactions are among the most plausible Earth-like catalytic processes that could operate in the interstellar medium, as their primary reactants (H_2 and CO) are the two most abundant molecular species in space. Moreover, FTT reactions are highly exergonic, producing a variety of complex organic molecules that have been detected in different astrophysical environments. Recent computational studies have explored possible reaction pathways for the formation of short-chain alcohols and alkanes via FTT reactions, using atomistic models of astrocatalysts of single-atom iron (Fe-SA) on a silica (SiO_2) surface (Fe-SA@SiO_2) (Pareras et al., 2023; Pareras et al., 2024). These studies provided mechanistic and kinetic insights of FTT processes, demonstrating the feasibility of synthesizing formaldehyde, methanol, methene, ketene, acetaldehyde, and ethanol in astrophysical environments where temperatures exceed 200 K. This theoretical framework offers, for the first time, insights how and where FTT-catalysed processes might take place in space. Moreover, seminal experiments dedicated to the synthesis of hydrocarbons catalysed by transition metal-containing dust analogues under simulated solar nebula conditions via FTT reactions demonstrate that true catalysis on cosmic grains can indeed occur (Llorca and Casanova, 1998; Ferrante et al., 2000; Sekine et al., 2006; Cabedo et al., 2021; Martinez-Bachs et al., 2024).

Here, accurate density functional theory (DFT) calculations on the catalytic potential of Fe-SA on SiC surfaces (Fe-SA@SiC) in the conversion of H_2 and CO in a FTT context are presented, with the focus on forming formaldehyde (H_2CO) and methanol (CH_3OH). The objective is to expand the understanding of astrocatalysis involving supported transition metals while leveraging the catalytic properties of SiC. This work aims to bridge the gap between the demonstrated efficiency of SiC materials in terrestrial catalysis and the established role of Fe-SA as effective catalysts in astrochemical processes. Ultimately, this study contributes to our understanding of how dust grains facilitate complex molecular formation in space, bridging astrochemical modelling with catalytic mechanisms relevant to both astrophysical and terrestrial chemistry.

2 Computational details

All the calculations were performed adopting a periodic approach and using the CP2K package (Kühne et al., 2020).

Characterization of the potential energy surface (PESs) requires determining the structures and the energetics of the stationary points. For geometry optimizations, the semi-local PBEsol functional (Perdew et al., 2008) was used, along with the Grimme's D3(BJ) (Grimme et al., 2010) correction to include dispersion forces. A double-ζ basis set (in CP2K, the DZVP-MOLOPT-SR-GTH gaussian basis set) (Vandevondele et al., 2005) was adopted for all the atom types, combined with a cut-off energy set at 500 Ry for the plane wave auxiliary basis set. The Goedecker–Teter–Hutter pseudopotentials (Goedecker et al., 1996) were used to describe core electrons, while a mixed Gaussian and plane-wave (GPW) approach (Lippert et al., 1997) was employed for valence electrons. The energies of the stationary points were refined by performing single point calculations onto the PBEsol-optimized geometries at the hybrid B3LYP functional (Becke, 1993) theory level, with the D3(BJ) dispersion correction (hereafter referred to as B3LYP-D3(BJ)//PBEsol-D3(BJ) theory level) and using the triple-ζ (TZVP) basis set (Lee et al., 1988). Note that the auxiliary density matrix method (ADMM) (Guidon et al., 2009; Guidon et al., 2010) was used for the exact exchange when performing calculations with hybrid functionals. The selection of B3LYP-D3(BJ) method for the energetic refinement was chosen because it was already benchmarked and used in our previous studies on astrocatalytical FTT reactions, (Pareras et al., 2023; Pareras et al., 2024; Martinez-Bachs et al., 2024), this way facilitating a consistent comparison. The choice of functionals and basis sets was based on calibration performed in our previous studies (Pareras et al., 2023; Pareras et al., 2024) on Fe single-atom systems, where it was demonstrated that the B3LYP-D3(BJ)/TZVP//PBEsol-D3(BJ)/DZVP approach provided the best agreement with CCSDT reference data in describing the electronic behaviour of the Fe centre.

The climbing image nudged elastic band (CI-NEB) (Zarkevich and Johnson, 2015) technique implemented in CP2K was used to search for transition states, which were also calculated at B3LYP-D3(BJ)//PBEsol-D3(BJ). Energy barriers were calculated as:

$$\Delta E^{\ddagger} = E_{TS} - E_{GS} \tag{1}$$

$$\Delta U^{\ddagger} = \Delta E^{\ddagger} - \Delta ZPE \tag{2}$$

$$\Delta G_T^{\ddagger} = \Delta E^{\ddagger} + \Delta G_T \tag{3}$$

where $\Delta E^{\ddagger}$ stands for the potential energy barrier (in which E_{TS} and E_{GS} refer to the absolute potential energies of the transition states and the previous local minima, respectively), $\Delta U^{\ddagger}$ represents the zero-point energy (ZPE) corrected barrier (in which ΔZPE refers to the contribution of the ZPE corrections to $\Delta E^{\ddagger}$), and $\Delta G_T^{\ddagger}$ is the Gibbs energy barrier at a given temperature (in which ΔG_T refers to the contribution of the Gibbs corrections to $\Delta E^{\ddagger}$).

The nature of the stationary points of the reactions was validated by calculating the harmonic frequencies (minima for reactants, intermediates and products, and first-order saddle points showing only one imaginary frequency for transitions states). Vibrational harmonic frequencies were calculated at the PBEsol-D3BJ/DZVP-optimized structures using the finite differences method as implemented in the CP2K code. To minimize the computational cost, a partial Hessian approach was employed. Consequently, vibrational frequencies were computed solely for a subset of the entire system, comprising the surface atoms participating in the reaction and the reactive species.

The catalytic performance of the simulated FTT processes was investigated through kinetic analyses. To this aim, a rate constant associated with each elementary barrier was calculated using the Rice-Ramsperger-Kassel-Marcus (RRKM) theory, (Marcus, 1952), a microcanonical transition state theory that assumes that the phase space is statistically populated. In this RRKM treatment, tunnelling effects were taken into account by adopting the unsymmetrical Eckart potential barrier model (Eckart, 1930). Calculation of the rate constants used the calculated vibrational frequencies as degrees of freedom in the sum of states. A partial Hessian matrix was calculated to derive a set of vibrational modes directly involved in the reaction, i.e., those that have a direct impact on the rate constants. The rest of the vibrational modes, not accounted for, belong to the inner layers of the surface model and are assumed to have a negligible influence in the chemical reactions and by extension in the rate constants (Molpeceres et al., 2023). These kinetic calculations were performed with a freely available in-house program, in which the RRKM algorithms were implemented for grain-surface processes (Enrique-Romero and Rimola, 2022).

3 Results and discussion

3.1 Atomistic model of the Fe^0@SiC catalyst

As previously mentioned, astronomical observations indicate that the most prevalent polymorph of silicon carbide in the interstellar medium is β-SiC. This phase adopts a zinc blende crystal structure (cubic unit cell) with an $F\bar{4}3m$ space group, where each Si atom is tetrahedrally coordinated by four equivalent C atoms, forming corner-sharing [SiC_4] tetrahedra, and vice-versa, each C atom is coordinated to four Si atoms, forming corner-sharing [Si_4C]. The bulk structure contains the $(SiC)_4$ minimal unit block and lattice parameters of a = b = c = 4.35 Å and α = β = γ = 90.00°, with uniform Si–C bond lengths of 1.89 Å. In this study, a supercell (2 × 2 × 2) model of the SiC bulk structure containing 64 atoms was employed. Upon optimization, the model exhibits lattice parameters of a = b = c = 8.68 Å and α = β = γ = 90.00°, with optimized Si–C bond lengths of 1.88 Å (Figure 1A). Following bulk optimization, various surface slabs were generated, corresponding to the Miller indices (100), (010), (001), (110), (011), (101), and (111). In order to identify the most stable slab, the surface energy for each of them was computed with the equation:

$$\mathrm{Y} = \frac{E_{slab}^{relaxed} - nE_{bulk}}{2A} \tag{4}$$

where (Y) is the surface energy, ($E_{slab}^{relaxed}$) is the energy for the relaxed structure of the slab, (n) are the number of atoms, (E_{bulk}) the energy of the bulk structure and (A) the surface area (Martinez-Bachs et al., 2024).

The surface energy values, calculated using Equation 4 and summarized in Table 1, indicate that the (110), (011) and (101) surfaces are the most stable ones. Since they are equivalent due to symmetry constraints, all the calculations were conducted using the (110) surface. The optimized structure of the slab (110) has optimized lattice parameters of a = 12.389, b = 8.717, c = 44.427 and

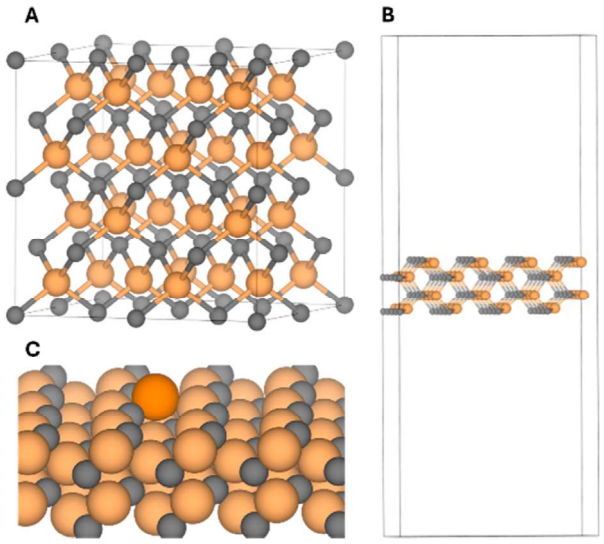

FIGURE 1
(A) Bulk structure of the β-SiC within a (2 × 2) supercell modelling. **(B)** Optimized structure of the (110) SiC slab model. **(C)** Zoom-in to the optimized structure of the Fe^0@SiC. Colour-coding: carbon atoms, grey; silicon atoms, ochre; iron atom, orange; unit cell, black lines.

α = β = γ = 90.00°, note that it has been set a vacuum of around 40 Å in order to assure isolation along the z direction (Figure 1B).

The Fe atom was incorporated on the (110) SiC surface, resulting in an optimized structure where Fe attaches to two undercoordinated C atoms and one undercoordinated Si atom, which are exposed to the outermost positions of the surface due to slab truncation (see Figure 1C). Note that, it has been chosen the high spin state for the Fe atom (quintet multiplicity) as based on our previous studies on Fe^0-SA it has been determined this as its electronic ground state (Sargent et al., 2009; Sasaki et al., 2001). The optimized Fe–C and Fe-Si bond lengths are 2.05 Å and 2.24 Å, respectively. Additionally, the introduction of Fe induces a slight structural reconstruction, shortening the nearby Si–C bonds by approximately 0.1 Å relative to the original Si–C bond length. An alternative coordination of the Fe atom involving two Si atoms and 1 C atom was also investigated (Supplementary Figure S1). This configuration was found to be 14.6 kcal mol^{-1} higher in energy than the most stable structure, where Fe is coordinated to 2 C atoms and one Si atom.

3.2 FTT-formaldehyde formation on Fe^0@SiC

Formaldehyde and methanol formation explored here follows a FTT reaction mechanism that involves the H_2 addition to CO. The precise mechanism of FT synthesis remains a topic of debate; however, in this study, we adopt an CO insertion-like mechanism (Figure 2). (Cabedo et al., 2021; Fischer and Tropsch, 1923; Fischer and Tropsch, 1926; Khodakov et al., 2007; De Smit and Weckhuysen, 2008; Cheng et al., 2010; Li et al., 2011; Foppa et al., 2016; Foppa et al., 2019) This choice is based on the assumption of minimal surface coverage, meaning that a single CO molecule is inserted and hydrogenated by one H_2 molecule at a time.

The mechanism begins with the adsorption of an H_2 molecule on the Fe-SA, as H_2 is significantly more abundant than CO. The potential energy surface (PES), calculated using Equations 1–3, as well as the optimized geometries of the reaction intermediates are depicted in Figure 3. Upon adsorption, partial activation of H_2 is observed, as evidenced by an elongation of the H–H bond to 0.92 Å (compared to its molecular bond length of 0.72 Å). Previous studies have reported that homolytic cleavage of H_2 facilitates subsequent CO hydrogenation (Foppa et al., 2019). Consequently, we evaluated the energetic cost of H_2 dissociation, finding an activation barrier of 4.8 kcal mol^{-1}, with a reaction energy of −17.2 kcal mol^{-1}. The stabilization of the dissociated H_2 product is attributed to the interaction of 1 H atom with a nearby Si atom. This structure forms a three-center two-electron bond, resembling a bridging hydride ligand, which adopts a characteristic bent geometry. Despite variations in bond lengths, the overall geometry of the optimized structure approximates a square pyramidal configuration (see structure [HH] in top Figure 3).

The next step involves the exergonic adsorption of CO, resulting in an optimized structure with a total energy of −41.4 kcal mol^{-1}. In this configuration, CO is coordinated to the metal center via the carbon atom, adopting a geometry close to octahedral (see structure [HH-CO] in top Figure 3). Coordination to the metal center partially activates CO, as indicated by the elongation of the C–O bond, from 1.15 Å in the gas phase to 1.17 Å in the Fe-bound structure.

Once both reactants are coordinated, the first hydrogenation step occurs, leading to the formation of the HCO intermediate ([HCO] structure in top Figure 3). This process overcomes a relative activation barrier of 15.2 kcal mol^{-1}, yielding HCO at an energy of −43.7 kcal mol^{-1}. Interestingly, this intermediate is 2.2 kcal mol^{-1} lower in energy than the preceding structure, indicating a slightly exergonic step.

The final hydrogenation step, leading to formaldehyde (H_2CO) formation has a slightly higher activation barrier of 18.3 kcal mol^{-1}. This increase in barrier height is attributed to the fact that the hydrogen atom involved in this step is initially part of the stable Fe–H–Si bridging structure. This elementary step is favorable with a reaction energy of −22.2 kcal mol^{-1}, and the overall formaldehyde formation being highly exergonic, with the final product situated at −65.9 kcal mol^{-1}.

The H_2CO moiety binds in an η^2-fashion, where both the carbon and oxygen atoms interact with the Fe center, with a C–O distance of 1.41 Å (see structure [H_2CO] in top Figure 3). The interaction of H_2CO with the Fe-SA presents a π-back-donation from Fe to the C=O antibonding orbital, which weakens the C=O bond. This interpretation is further supported by analysis of the calculated Mulliken charges (Supplementary Tables S1, S2), which shows an increase in the positive charge on the Fe centre from +0.1783 in [HCO] to +0.3890 in [H_2CO], indicating electron donation. Concurrently, the C and O atoms in H_2CO reduce their charges, consistent with π-back-donation. The geometry also reveals a slight bending of H_2CO toward a nearby Si atom, with an O··Si distance of 1.80 Å, and Mulliken charges of −0.3585 (O) and +0.9133 (Si), supporting the presence of a weak O··Si interaction. Interestingly, along the reaction path, the Fe-SA presents some mobility around its

TABLE 1 Miller indices of the SiC plane surfaces considered in this work including their surface areas (in Å), calculated surface energies (ϒ, in (J m^{-2}), the n values, the optimized cell parameters (in Å), and the thickness of the slab models (in Å).

Miller indices	Surface area	n	Y	Cell parameters			Thickness
				a	b	c	
(100)	72.19	1.00	3.64	8.497	8.495	47.674	8.34
(010)	75.23	1.00	5.23	8.674	8.673	47.524	7.75
(001)	75.23	1.00	5.23	8.674	8.674	47.524	8.34
(110)	108.00	1.00	3.21	12.389	, 8.717	44.427	4.73
(011)	108.00	1.00	3.21	8.717	12.389	44.427	4.73
(101)	108.00	1.00	3.21	12.389	8.717	44.427	4.73
(111)	149.70	2.00	3.64	12.193	12.277	49.179	9.40

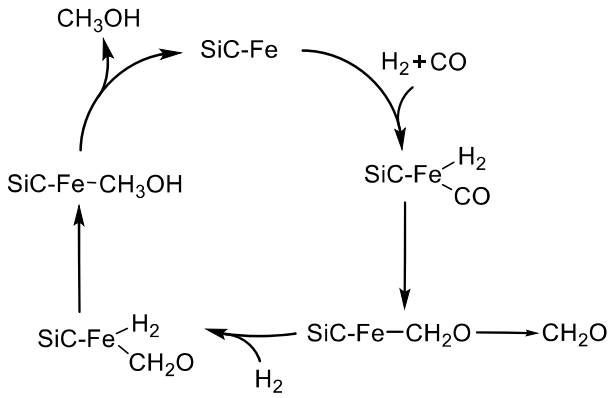

FIGURE 2
Proposed catalytic cycle for the formaldehyde and methanol formation catalysed by Fe^0@SiC.

binding site, indicating that, although it is adsorbed on the surface, it exhibits slight freedom of movement, which facilitates a smoother reaction process.

3.3 FTT-methanol formation on Fe^0@SiC

A second PES relative to methanol formation has been characterized (shown in Figure 4 alongside the optimized geometries of the reaction intermediates), assuming as zeroth reference the optimized [H_2CO] intermediate. The mechanism starts with the insertion of a second H_2 molecule coordinating the metal center. The introduction of this second H_2 molecule stabilizes the intermediate, yielding a relative energy of −14.8 kcal mol^{-1}. However, this adsorption induces a significant structural reorganization around the Fe-SA due to the occupancy of the metal site, in which the H_2CO moiety loses its η^2-coordination mode. That is, in the optimized structure the carbon atom remains attached to the metal center, while the oxygen now bonds to an undercoordinated Si atom of the surface, which is driven by the complementarity of the charge densities of the two atoms (positive for Si; negative for O). As a result, the C=O bond elongates to 1.40 Å.

The next step involves the formation of the H_3CO intermediate. Note that in our previous works, the formation of CH_2OH was also considered. However, this pathway showed a significantly higher energy barrier compared to the formation of CH_3O (Pareras et al., 2023; Pareras et al., 2024). Previous studies suggest that the formation of H_3CO (namely, hydrogenation of the C atom) is energetically more favorable than formation of H_2COH (namely, hydrogenation of the O atom) (Pareras et al., 2023; Van Der Laan and Beenackers, 1999; Foppa et al., 2018; Wu et al., 2011). Here, a stepwise mechanism is considered, where H_2 first undergoes a homolytic cleavage, followed by the hydrogenations. The H_2 dissociation barrier is 11.4 kcal mol^{-1}, yielding an endergonic intermediate of 7.2 kcal mol^{-1} with respect to the pre-reactant complex. As seen before, one hydrogen atom forms a bridging bond between the Fe-SA center and a nearby Si atom. The first hydrogenation of H_2CO to form H_3CO has an activation barrier as low as 3.4 kcal mol^{-1}, but 2.4 kcal mol^{-1} endergonic with respect to the previous intermediate.

The optimized H_3CO structure (see [H_3CO] in top Figure 4) shows that the H_3CO moiety forms a bridging bond with its O atom, a Si surface atom and the Fe-SA. This structure appears relatively stable, as the subsequent hydrogenation step leading to methanol formation has a high activation barrier of 32.6 kcal mol^{-1}, the highest one in the pathway. Moreover, the final methanol product is at 2.5 kcal mol^{-1} above the initial state, indicating an overall endergonic reaction.

To sum up, formaldehyde formation proceeds smoothly, with the highest activation barrier reaching 18.3 kcal mol^{-1} and the entire process being exergonic, a crucial characteristic for reactions occurring in the ISM, where energy sources are limited. However, further hydrogenation to methanol is more energetically demanding. While the formation of the H_3CO intermediate involves relatively low energy barriers, the final step forming methanol is characterized by a large energy barrier (32.6 kcal mol^{-1}) and the overall reaction energy is endergonic. These energetic features

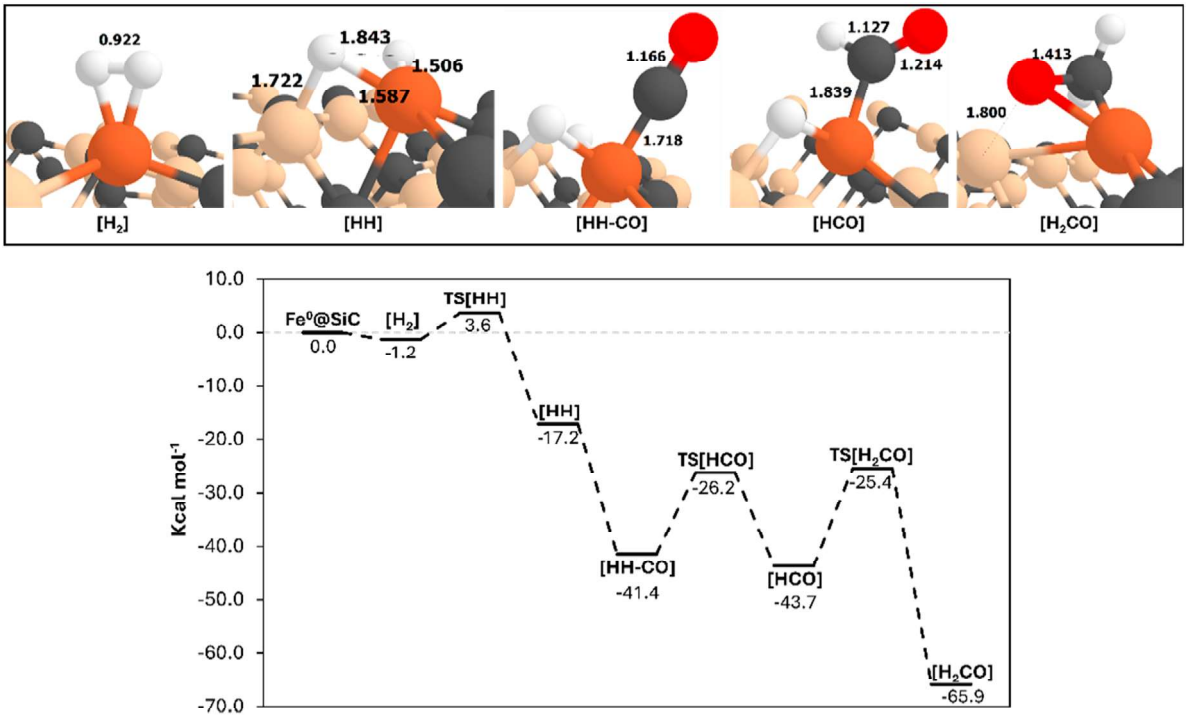

FIGURE 3
Top: PBEsol-B3 (DJ)-optimized geometries of the minima stationary points of the PES leading to formaldehyde formation. bottom: ZPE-corrected PESs (in kcal mol^{-1}) for the formaldehyde formation, using as the 0th reference energy the Fe^0@SiC asymptote. Bond distances are in Å. Colour-coding: carbon atoms, grey; silicon atoms, ochre; iron atom, orange.

can be correlated with structural rearrangements of the Fe-SA along the reaction, more particularly playing a crucial role in stabilizing intermediates. That is, through the formation of Fe–H–Si bridging bonds, the H_2 cleavage and subsequent CO hydrogenation is facilitated. However, this same flexibility restricts the final step, as the bridging bonds formed by the Fe-O–Si and Fe-H–Si create a highly stable configuration that imposes a high energy barrier for methanol formation. The catalytic role of the Fe centre is evidenced by its ability to promote the homolytic cleavage of H_2, thereby facilitating subsequent hydrogenation steps, and by its activation of the CO molecule, as demonstrated by the elongation of the C–O bond upon coordination. These two effects are essential, as the direct hydrogenation of CO by H_2 in the absence of a catalyst would be energetically inaccessible.

3.4 Kinetic analysis

The mechanistic study presented above provides valuable insights into the most energetically feasible pathways and reveals how interactions and structural rearrangements influence the reactivity. Here, the reaction kinetics using the RRKM theory, including tunnelling effects, is analysed, which allows estimating the temperature ranges at which these processes can occur, and accordingly those astrophysical environments where they are feasible within the broader context of planetary formation. To this end, for each elementary step, the temperatures at which the rate constants are close to 1 year^{-1}. The choice of this approximated reaction constant threshold is based on the fact that the half-times of interstellar molecular clouds range from 1 to 10 Myears, the rate constants thus aligning well with these astronomical timescales.

Computed kinetic data are summarized in Table 2. The first reaction step, which involves homolytic cleavage of H_2, shows a significant tunneling effect. The reaction constant considering tunnelling (k_{tun}) in astronomical units, years^{-1} (yr^{-1}), shows already a k = 4.16 yr^{-1} at a temperature of 7 K, suggesting that despite the presence of an energy barrier, this step can be considered effectively barrierless due to hydrogen atom tunneling. This implies that the homolytic cleavage of H_2 on Fe^0@SiC occurs spontaneously. The next step, leading to the formation of the HCO intermediate, presents a different scenario. Here, the activation barrier is relatively higher, and despite the reaction being exergonic with a reaction energy of −2.2 kcal mol^{-1}, the calculated classical rate constant (k) is 1.23 yr^{-1} at 165 K, with tunneling effects being negligible. This indicates that, while a certain level of thermal energy is necessary, the reaction remains feasible in cold-warm astrophysical environments. The final hydrogenation step leading to formaldehyde formation exhibits an activation barrier of approximately 18 kcal mol^{-1}, moreover it is highly exergonic with a reaction energy of −22.2 kcal mol^{-1}. As expected, a rate constant k = 1.07 years^{-1} is reached at 199 K. In this case, tunneling does not significantly reduce the temperature requirements.

Following the proposed reaction mechanism, a second H_2 molecule adsorbs onto the surface before formaldehyde hydrogenation, forming the H_3CO intermediate. Unlike the previous H_2 homolytic cleavage, this process involves an activation

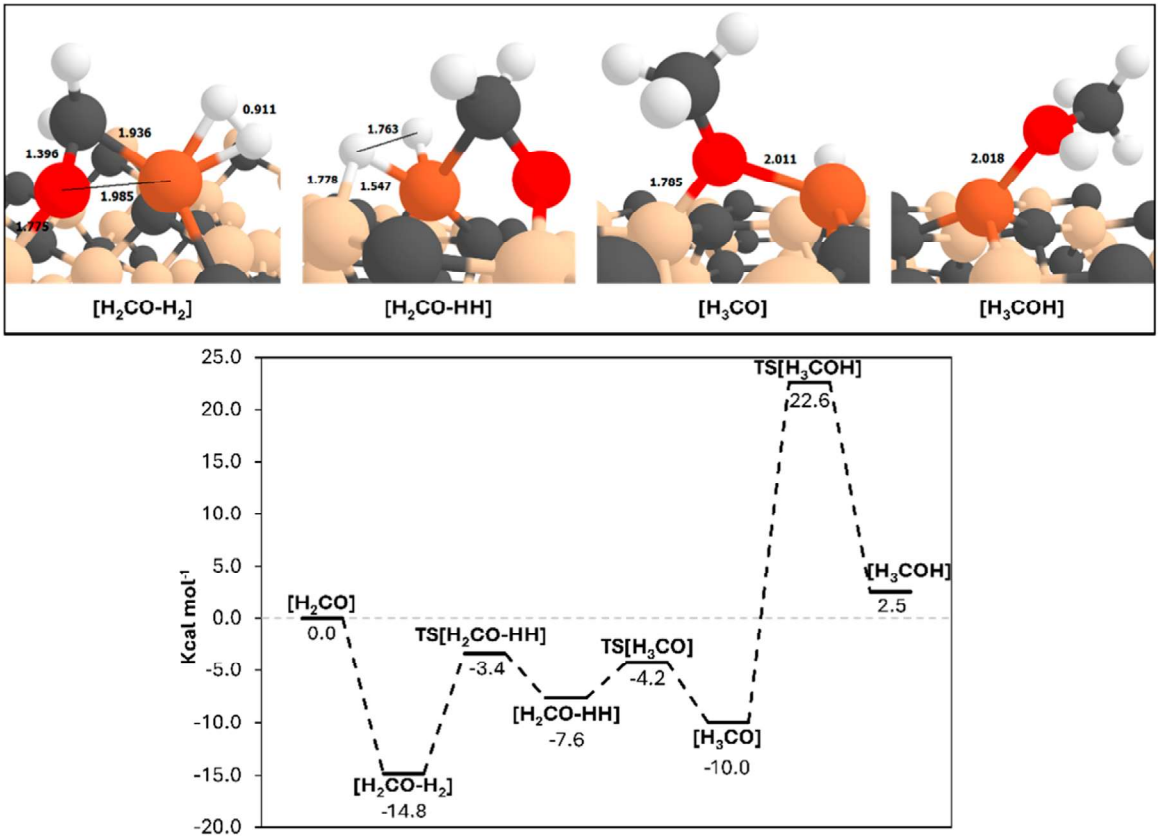

FIGURE 4
Top: PBEsol-B3 (DJ)-optimized geometries of the minima stationary points of the PES leading to methanol formation. bottom: ZPE-corrected PESs (in kcal mol^{-1}) for the formaldehyde formation, using as the 0th reference energy the Fe^0@SiC-[H2CO] asymptote. Bond distances are in Å. Colour-coding: carbon atoms, grey; silicon atoms, ochre; iron atom, orange.

TABLE 2 Represented the ZPE-corrected energy barriers ($\Delta U^{\ddagger}$) and reaction energies (ΔU_{Rx}), the calculated classical rate constants (k) and tunnelling rate constants (k_{tun}) both in years^{-1} (yr^{-1}) and the associated temperatures (T) in Kelvins (K) for all the elementary steps involved in the formaldehyde and methanol formation mechanisms.

Mechanism	Elementary steps	$\Delta U^{\ddagger}$	ΔU_{Rx}	k (yr^{-1})	T (K)	k_{tun} (yr^{-1})	T_{tun} (K)
Formaldehyde Formation	TS [HH]	4.8	−15.9	2.28	55	4.16	7
	TS [HCO]	15.2	−2.2	1.23	165	1.03	164
	TS [H_2CO]	18.3	−22.2	1.07	199	1.21	197
Methanol Formation	TS [H_2CO-HH]	11.4	7.2	1.27	126	-	-
	TS [H_3CO]	3.4	−2.4	1.46	38	1.22	4
	TS [H_3COH]	32.6	12.5	1.01	347	-	-

barrier of 11.4 kcal mol^{-1} and is endergonic, with a reaction energy of 7.2 kcal mol^{-1}. This corresponds to a rate constant k = 1.27 yr^{-1} at 126 K. Although energy input is required for H_2 cleavage, this facilitates subsequent H_2CO hydrogenation, which exhibits a low barrier of 3.4 kcal mol^{-1} and an exergonic reaction energy of −2.4 kcal mol^{-1}. In kinetic terms, this step achieves a K_{tun} = 1.22 s^{-1} at 4 K. This suggests that, despite the presence of an energy barrier, H_2CO hydrogenation can be considered effectively spontaneous once H_2 cleavage has occurred. The final hydrogenation step leading to methanol formation is the most challenging, with a substantial energy barrier and an endergonic character. Kinetic data indicates that this step is not feasible in cold-warm regions, as a significant energy input is required. A rate constant of k = 1.01 s^{-1} is not reached until 347 K. This suggests that methanol formation is significantly restricted under typical ISM conditions.

3.5 Astrophysical implications

The theoretical data presented in this study aims to predict the catalytic formation of formaldehyde and methanol via a FTT mechanism in astrophysical environments. A key question, however, is how these values align with observational data and under what conditions these processes are feasible.

As mentioned in the introduction, SiC has been consistently observed in outer space, however, it has not yet been detected in the ISM and has only been identified in regions beyond the protoplanetary disk stage. While this limitation might initially seem like a drawback, it actually reinforces the plausibility of the proposed mechanism. The Fe^0@SiC-catalyzed formaldehyde/methanol formation processes require a minimum temperature threshold, making it more likely to occur in "warm" environments, such as protoplanetary disks, where temperatures are sufficiently high. Therefore, the proposed reaction is not feasible in deep cold regions of the ISM such as dense molecular clouds, mainly due to the high energy barriers involved alongside the fact that SiC are usually present in planetary formation late-stages.

This raises the question of how our reaction mechanism fits into the broader context of planetary system formation. The kinetic data indicates that the first hydrogenation steps leading to formaldehyde formation require temperatures of at least 200 K, while the final methanol formation is more restrictive, requiring temperatures of at least 347 K. Consequently, these reactions are likely to occur in regions out of the coldest parts of protoplanetary disks. Another important consideration is whether the reactants and intermediates remain coordinated to the Fe atom at the temperatures required to overcome the computed barriers. Thus, it is necessary to compare these temperatures with those at which the reactants can desorb. To do that, we estimate the desorption temperature of the reactants (T_{des}) as follows, adopting a similar procedure as reported by some of us (Bariosco et al., 2025) On one hand, we first consider the half-life time ($\tau_{1/2}$) of the species in the environment (consistently assumed to be 10^6 years) and its relationship to the thermal desorption rate (k_{des}) as (first order desorption):

$$\tau_{1/2} = \frac{ln(2)}{k_{des}} \quad (5)$$

On the other hand, the thermal desorption rate of a species bound to a substrate can be approximately described by the Polanyi–Wigner equation, (Polanyi and Wigner, 1928), the expression of which for first order desorption is:

$$k_{des} = \nu_{des} e^{\left(-\frac{BE}{T_{des}}\right)} \quad (6)$$

where ν_{des} is the thermal desorption pre-exponential factor and BE the binding energy of the species on the substrate. Combining Equations 5, 6, 7 to derive T_{des} estimates:

$$T_{des} = \frac{BE}{ln(\nu_{des}) - ln(k_{des})} \quad (7)$$

where BE is given in K, and ν_{des} and k_{des} in s^{-1}

In our previous studies on Fe single-atom systems, (Pareras et al., 2023; Pareras et al., 2024), we computed the binding energies of H_2, CO, H_2CO, and CH_3OH to be 34.6, 41.39, 74.0, and 58.39 kcal mol^{-1}, respectively, all of which higher than the activation barriers reported here. Furthermore, by applying Equation 7, the corresponding T_{des} are 239 K for H_2, 286 K for CO, 510 K for H_2CO, and 403 K for CH_3OH. In every case, the T_{des} values exceed the temperatures at which the activation barriers can be overcome. This ensures that once H_2 and CO are coordinated to the Fe center, they will remain adsorbed long enough to react and form H_2CO. Subsequently, H_2CO will also stay bound to the Fe site, enabling further reaction to produce CH_3OH, even at the highest temperature involved in the process (347 K), required for the final step.

Protoplanetary disks (PDs), the birthplaces of planetary systems, contain a wide range of chemical species crucial for planet formation. Formaldehyde and methanol are primarily observed in the disk midplane, (Walsh et al., 2016; Podio et al., 2019; Öberg et al., 2017; Qi et al., 2013), where temperatures range from tens to hundreds of Kelvins, within ~100 AU from the central star.

The identification of SiC in PDs is challenging due to their optically thick nature, which limits high-resolution observations. Nonetheless, tentative detections in young stellar environments exist (Saikia et al., 2019). SiC is also found in carbon star outflows (McCarthy et al., 2019) and, although rarely observed in the ISM, possibly due to mixing with small carbonaceous grains, (Jones et al., 2013), models estimate that up to 25% of refractory carbon may be in the form of SiC (Li et al., 2002). Similarly, Fe-bearing species such as FeS (Keller et al., 2002) and solid iron grains (Varga et al., 2024) have been detected in PDs. Fe is also incorporated into silicates during later formation stages, likely via vapor deposition and insertion, (Woitke, 2006), a process that could similarly apply to SiC. These findings suggest that SiC and Fe, and potentially Fe@SiC systems, may indeed be present in PD environments.

Disk chemistry models point out that these species may be formed by gas-phase processes close to the star and by cold grain surface processes followed by non-thermal desorption in the outer disk, yet current astrochemical models struggle to explain their observed abundances, particularly methanol, as model predictions often fail to reconcile observational values by several orders of magnitude (Walsh et al., 2017).

Here we propose that grain surface chemistry can occur even beyond the snowline, in the warm regions of the inner disk, in which ices have already sublimated but refractory dust grains still reside. Investigated FTT processes do not occur on ice mantles but on refractory materials, in this case of SiC with Fe-SA attached on the surface. The adsorption of H_2 (in a dissociative mode) and of CO on the Fe-SA center is indeed highly favorable, thus assuring a stable adsorption complex of these species even at high temperatures. Our kinetic analysis indicate that H_2CO can be significantly formed at temperatures higher than 200 K, and CH_3OH higher than 350 K, which are temperatures easily to reach in the inner disk regions containing "rocky" dust grains. Thus, in these regions, in addition to gas-phase processes, the FTT reactions investigated here can well take place, feeding their H_2CO and CH_3OH content and providing a likely missing methanol source under inner disk conditions.

Formaldehyde and methanol have also been detected in comets, likely originating from earlier planetary formation phases and the ices of primitive dust grains (Hoban et al., 1991; Reuter, 1992; Davies et al., 1993; Eberhardt' et al., 1994; Altwegg et al., 2016; Rubin et al., 2019). Their abundances are expected to vary depending on the protoplanetary disk region and environmental factors such as temperature, CO depletion, and irradiation conditions (Faggi et al., 2023; Llorca, 2002). Although no direct evidence exists for FTT reactions in comets, depending on the above-mentioned conditions,

formaldehyde and methanol identified in comets could also be formed through the investigated FTT processes, Moreover, the occurrence of FTT can be extended to other cometary organic molecules, such as ethylene (CH_2 = CH_2), the presence of which in comets remains unexplained and could be linked to FTT chemistry (Dart and ois, 2021).

FTT reactions may also play a role in planetary atmospheres. Protoplanets can efficiently accumulate H_2 from the protoplanetary nebula, which is also rich in CO. In such environments, catalytic Fe-containing inclusions, possibly delivered via chondritic meteoritic material, combined with elevated temperatures could promote FTT reactions, leading to the formation of alcohols and hydrocarbons (Stökl et al., 2016; Lamm et al., 2018; Kress and McKay, 2004).

Finally, it is crucial to recognize that the FT process is not limited to formaldehyde and methanol production. It is a polymeric-like mechanism that predominantly forms short-chain alkanes and alkenes. Our findings suggest that, at intermediate temperatures, formaldehyde formation is feasible, whereas methanol formation is energetically restricted. This opens the possibility of a complex network of hydrocarbon formation, including ketene, acetaldehyde, and other alkanes and alkenes.

4 Conclusion

This study provides a comprehensive theoretical investigation into the catalytic formation of formaldehyde and methanol on Fe^0@SiC surfaces via a FTT mechanism in astrophysical environments. Our results demonstrate that the β-SiC (110) surface, when doped with Fe-SA, serves as an effective catalyst for the hydrogenation of CO and H_2, key abundant reactants in space. Formaldehyde formation proceeds efficiently, with low activation barriers (up to 18.3 kcal mol^{-1}) and an exergonic behaviour, further enhanced by hydrogen tunnelling effects that enable kinetically reactions at temperatures of ~200 K. In contrast, methanol formation encounters a significant energy barrier (32.6 kcal mol^{-1}), making it less favourable under interstellar conditions. The stability of Fe-O-Si and Fe-H-Si bridging interactions plays a crucial role in stabilizing intermediates, facilitating formaldehyde synthesis but hindering methanol production.

The astrophysical implications of our findings suggest that Fe_0@SiC-catalyzed FTT reactions are most relevant in environments with moderate thermal energy, where temperatures align with the predicted thresholds for these reactions. This would be the case of warm inner planes of protoplanetary disks, beyond ice snow lines, in which ices have sublimated and where bare refractory dust grains still reside and could explain the observed abundances of formaldehyde and methanol in such regions, particularly for methanol as disk chemistry models fail to reproduce the observed abundances. Additionally, our study highlights the potential role of catalytic Fe-containing inclusions in driving hydrocarbon formation within planetary atmospheres and cometary bodies, offering new insights into the chemical evolution of planetary systems. Beyond methanol, the FTT process may extend to the formation of other organic molecules, including short-chain alkanes, alkenes, ketene, and acetaldehyde, suggesting a broader network of hydrocarbon chemistry in space.

5 Associated content

The computational data sets presented in this study is open sourced at the CORA database (https://doi.org/10.34810/data2153). In the online repository are collected, the SiC slab in CIF format, all the geometries in XYZ format, the vibration outputs, examples of the different inputs and outputs and all the kinetic values.

Data availability statement

The datasets presented in this study can be found in online repositories. The names of the repository/repositories and accession number(s) can be found in the article/Supplementary Material.

Author contributions

GP: Software, Writing – original draft, Visualization, Formal Analysis, Methodology, Conceptualization, Resources, Validation, Data curation, Investigation, Writing – review and editing. AR: Funding acquisition, Project administration, Writing – review and editing, Visualization, Validation, Resources, Conceptualization, Supervision.

Funding

The author(s) declare that financial support was received for the research and/or publication of this article. AR acknowledges funding within the European Union's Horizon 2020 research and innovation program from the European Research Council (ERC) for the project *Quantum Chemistry on Interstellar Grains* (QUANTUMGRAIN), grant agreement No 865657. GP and AR acknowledges the European Union's Horizon Europe research and innovation programme under the Marie Sklodowska-Curie grant agreement No. 101105235 for the funding for the project *Computational Studies on Heterogeneous Astrocatalysis of Space-Abundant Transition Metals* (CHAOS). GP thankfully acknowledges financial support by the Spanish Ministry of Universities and the European Union's Next-Generation EU fund for a Margarita Salas contract. Spanish MICINN is also acknowledged for funding the projects PID 2021-126427NB-I00 and CNS 2023-144902. The authors thankfully acknowledge RES resources provided by Univ. Valencia for the use of Tirant (activity QHS-2022-2-0022) and by BSC for the use of MareNostrum (activity QHS-2023-1-0019). We also thankfully acknowledge the computer resources and assistance provided by CSUC. AR gratefully acknowledges support through 2023 ICREA Award.

Conflict of interest

The authors declare that the research was conducted in the absence of any commercial or financial relationships that could be construed as a potential conflict of interest.

The author(s) declared that they were an editorial board member of Frontiers, at the time of submission. This had no impact on the peer review process and the final decision.

Generative AI statement

The author(s) declare that no Generative AI was used in the creation of this manuscript.

Publisher's note

All claims expressed in this article are solely those of the authors and do not necessarily represent those of their affiliated organizations, or those of the publisher, the editors and the reviewers. Any product that may be evaluated in this article, or claim that may be made by its manufacturer, is not guaranteed or endorsed by the publisher.

Supplementary material

The Supplementary Material for this article can be found online at: https://www.frontiersin.org/articles/10.3389/fspas.2025.1605553/full#supplementary-material

References

Altobelli, N., Postberg, F., Fiege, K., Trieloff, M., Kimura, H., Sterken, V. J., et al. (2016). Flux and composition of interstellar dust at saturn from cassini's cosmic dust analyzer. *Science* 352, 312–318. doi:10.1126/science.aac6397

Altwegg, K., Balsiger, H., Bar-Nun, A., Berthelier, J. J., Bieler, A., Bochsler, P., et al. (2016). Prebiotic chemicals-amino acid and phosphorus in the coma of comet 67P/Churyumov-Gerasimenko. *Sci. Adv.* 2, e1600285. doi:10.1126/sciadv.1600285

Ba, H., Liu, Y., Mu, X., Doh, W. H., Nhut, J. M., Granger, P., et al. (2015). Macroscopic nanodiamonds/β-SiC composite as metal-free catalysts for steam-free dehydrogenation of ethylbenzene to styrene. *Appl. Catal. A Gen.* 499, 217–226. doi:10.1016/j.apcata.2015.04.022

Bariosco, V., Tinacci, L., Pantaleone, S., Ceccarelli, C., Rimola, A., and Ugliengo, P. (2025). Gaseous methanol in cold environments: is thermal desorption from low binding energy sites the explanation? *Mon. Not. R. Astron. Soc.* 539, 82–94. doi:10.1093/mnras/staf476

Becke, A. D. (1993). A new mixing of Hartree-Fock and local density-functional theories. *J. Chem. Phys.* 98, 1372–1377. doi:10.1063/1.464304

Bernal, J. J., Zega, T. J., and Ziurys, L. M. (2022). Destructive processing of silicon carbide grains: experimental insights into the formation of interstellar fullerenes and carbon nanotubes. *J. Phys. Chem. A* 126, 5761–5767. doi:10.1021/acs.jpca.2c01441

Bhatnagar, M., and Baliga, B. J. (1993). Comparison of 6H-SiC, 3C-SiC, and Si for power devices. *IEEE Trans. Electron Devices* 40, 645–655. doi:10.1109/16.199372

Bradley, J. P. (1994). Chemically anomalous, preaccretionally irradiated grains in interplanetary dust from comets. *Science* 265, 925–929. doi:10.1126/science.265.5174.925

Brown, J. M., Körsgen, H., Beaton, S. P., and Evenson, K. M. (2006). The rotational and fine-structure spectrum of FeH, studied by far-infrared laser magnetic resonance. *J. Chem. Phys.* 124, 234309. doi:10.1063/1.2198843

Cabedo, V., Llorca, J., Trigo-Rodriguez, J. M., and Rimola, A. (2021). Study of Fischer-Tropsch-type reactions on chondritic meteorites. *Astron. Astrophys.* 650, A160. doi:10.1051/0004-6361/202039991

Carelli, F., Sebastianelli, F., Satta, M., and Gianturco, F. A. (2011). Gas-phase route to polycyclic aromatic hydrocarbon formation in protoplanetary atmospheres: role of stabilized benzyne anions. *Mon. Not. R. Astron. Soc.* 415, 425–430. doi:10.1111/j.1365-2966.2011.18711.x

Chen, T., Xiao, C. Y., Li, A., and Zhou, C. T. (2022). Where have all the interstellar silicon carbides gone? *Mon. Not. R. Astron. Soc.* 509, 5231–5236. doi:10.1093/mnras/stab3175

Cheng, J., Hu, P., Ellis, P., French, S., Kelly, G., and Lok, C. M. (2010). Some understanding of fischer-tropsch synthesis from density functional theory calculations. *Top. Catal.* 53, 326–337. doi:10.1007/s11244-010-9450-7

Cherchneff, I. (2011). The formation of Polycyclic Aromatic Hydrocarbons in evolved circumstellar environments, *EAS Publications Series EDP Sciences*, 46. 177–189. doi:10.1051/eas/1146019

Church, T. L., Fallani, S., Liu, J., Zhao, M., and Harris, A. T. (2012). Novel biomorphic Ni/SiC catalysts that enhance cellulose conversion to hydrogen. *Catal. Today* 190, 98–106. doi:10.1016/j.cattod.2012.01.041

Clement, D., Mutschke, H., Klein, R., and Henning, T. (2003). New laboratory spectra of isolated β-SiC nanoparticles: comparison with spectra taken by the infrared space observatory. *Astrophys. J.* 594, 642–650. doi:10.1086/376864

Cole, J. A., Bittner, J. D., Longwell, J. P., and Howard, J. B. (1984). Formation mechanisms of aromatic compounds in aliphatic flames. *Combust. Flame* 56, 51–70. doi:10.1016/0010-2180(84)90005-1

Dartois, E. (2021). Infrared spectroscopy of clathrate hydrates for planetary science: the ethylene case. *Mon. Not. R. Astron. Soc.* 504, 4369–4376. doi:10.1093/mnras/stab1083

Davies, J. K., Mumma, M. J., Reuter, D. C., Hoban, S., Weaver, H. A., Puxley, P. J., et al. (1993). The infrared (3.2-3.6 m) spectrum of comet P/Swift-Tuttle: detection of methanol and other organics. *Mon. Not. R. Astron. Soc.* 265, 1022–1026. doi:10.1093/mnras/265.4.1022

Delaunay, R., Gatchell, M., Rousseau, P., Domaracka, A., MacLot, S., Wang, Y., et al. (2015). Molecular growth inside of polycyclic aromatic hydrocarbon clusters induced by ion collisions. *J. Phys. Chem. Lett.* 6, 1536–1542. doi:10.1021/acs.jpclett.5b00405

De Smit, E., and Weckhuysen, B. M. (2008). The renaissance of iron-based Fischer-Tropsch synthesis: on the multifaceted catalyst deactivation behaviour. *Chem. Soc. Rev.* 37, 2758–2781. doi:10.1039/b805427d

Eberhardt, P., Meier, R., Krankowsky, D., and Hodges, R. R. (1994). Methanol and hydrogen sulfide in comet P/Halley. *Astron. Astrophys.* 288, 315–329.

Eckart, C. (1930). The penetration of a potential barrier by electrons. *Phys. Rev.* 35, 1303–1309. doi:10.1103/physrev.35.1303

Enrique-Romero, J., and Rimola, A. QuantumGrain RRKM code. (2022). doi:10.5281/ZENODO.10518616

Faggi, S., Lippi, M., Mumma, M. J., and Villanueva, G. L. (2023). Strongly depleted methanol and hypervolatiles in comet C/2021 A1 (leonard): signatures of interstellar chemistry? *Planet. Sci. J.* 4, 8. doi:10.3847/psj/aca64c

Ferrante, R. F., Moore, M. H., Nuth, J. A., and Smith, T. (2000). Laboratory studies of catalysis of CO to organics on grain analogs. *Icarus* 145, 297–300. doi:10.1006/icar.2000.6350

Fischer, F., and Tropsch, H. (1923). Uber die Herstellung synthetischer olgemische (Synthol) durch Aufbau aus Kohlenoxyd und Wasserstoff. *Brennst. Chem.* 4, 276–285. doi:10.1002/cber.19230561119

Fischer, F., and Tropsch, H. (1926). Über einige Eigenschaften der aus Kohlenoxyd bei gewöhnlichem Druck hergestellten synthetischen Erdöl-Kohlenwasserstoffe. *Eur. J. Inorg. Chem.* 59, 923–925. doi:10.1002/cber.19260590513

Fonfria, J. P., Cernicharo, J., Richter, M. J., and Lacy, J. H. (2008). A detailed analysis of the dust formation zone of IRC +10216 derived from mid-infrared bands of C 2 H 2 and HCN. *Astrophys. J.* 673, 445–469. doi:10.1086/523882

Foppa, L., Copéret, C., and Comas-Vives, A. (2016). Increased back-bonding explains step-edge reactivity and particle size effect for CO activation on Ru nanoparticles. *J. Am. Chem. Soc.* 138, 16655–16668. doi:10.1021/jacs.6b08697

Foppa, L., Iannuzzi, M., Copéret, C., and Comas-Vives, A. (2018). Adlayer dynamics drives CO activation in Ru-catalyzed fischer-tropsch synthesis. *ACS Catal.* 8, 6983–6992. doi:10.1021/acscatal.8b01232

Foppa, L., Iannuzzi, M., Copéret, C., and Comas-Vives, A. (2019). Facile fischer-tropsch chain growth from CH2 monomers enabled by the dynamic CO adlayer. *ACS Catal.* 9, 6571–6582. doi:10.1021/acscatal.9b00239

Frenklach, M., and Feigelson, E. D. (1989). Formation of polycyclic aromatic hydrocarbons in circumstellar envelopes. *Astrophys. J.* 341, 372. doi:10.1086/167501

Fujiyoshi, T., Wright, C. M., and Moore, T. J. T. (2015). Mid-infrared spectroscopy of SVS13: silicates, quartz and SiC in a protoplanetary disc. *Mon. Not. R. Astron. Soc.* 451, 3371–3384. doi:10.1093/mnras/stv1171

Gobrecht, D., Cherchneff, I., Sarangi, A., Plane, J. M. C., and Bromley, S. T. (2016). Dust formation in the oxygen-rich AGB star Ik Tauri. *Astron. Astrophys.* 585, 6. doi:10.1051/0004-6361/201425363

Goedecker, S., Teter, M., and Hutter, J. (1996). Separable dual-space Gaussian pseudopotentials. *Phys. Rev. B - Condens. Matter Mater. Phys.* 54, 1703–1710. doi:10.1103/physrevb.54.1703

Goel, A., Howard, J. B., and Sande, J. B. V. (2004). Size analysis of single fullerene molecules by electron microscopy. *Carbon N. Y.* 42, 1907–1915. doi:10.1016/j.carbon.2004.03.022

Grimme, S., Antony, J., Ehrlich, S., and Krieg, H. (2010). A consistent and accurate *ab initio* parametrization of density functional dispersion correction (DFT-D) for the 94 elements H-Pu. *J. Chem. Phys.* 132, 154104. doi:10.1063/1.3382344

Guidon, M., Hutter, J., and VandeVondele, J. (2009). Robust periodic Hartree-Fock exchange for large-scale simulations using Gaussian basis sets. *J. Chem. Theory Comput.* 5, 3010–3021. doi:10.1021/ct900494g

Guidon, M., Hutter, J., and Vandevondele, J. (2010). Auxiliary density matrix methods for Hartree-Fock exchange calculations. *J. Chem. Theory Comput.* 6, 2348–2364. doi:10.1021/ct1002225

Herrero, V. J., Jiménez-Redondo, M., Peláez, R. J., Maté, B., and Tanarro, I. (2022). Structure and evolution of interstellar carbonaceous dust. Insights from the laboratory. *Front. Astron. Sp. Sci.* 9, 1083288. doi:10.3389/fspas.2022.1083288

Hoban, S., Mumma, M., Reuter, D. C., DiSanti, M., Joyce, R. R., and Storrs, A. (1991). A tentative identification of methanol as the progenitor of the 3.52-μm emission feature in several comets. *Icarus* 93, 122–134. doi:10.1016/0019-1035(91)90168-s

Hoppe, P. (2009). Stardust in meteorites and IDPs current status, recent advances, and future prospects. *Cosm. DUST - NEAR FAR*, 414, 148–156.

Ishii, H. A., Bradley, J. P., Bechtel, H. A., Brownlee, D. E., Bustillo, K. C., Ciston, J., et al. (2018). Multiple generations of grain aggregation in different environments preceded solar system body formation. *Proc. Natl. Acad. Sci. U. S. A.* 115, 6608–6613. doi:10.1073/pnas.1720167115

Jones, A. (2001). "Dust in the dense interstellar medium," in *From darkness to light: origin and evolution of young stellar clusters*, 243 37.

Jones, A. P., Fanciullo, L., Köhler, M., Verstraete, L., Guillet, V., Bocchio, M., et al. (2013). The evolution of amorphous hydrocarbons in the ISM: dust modelling from a new vantage point. *Astron. Astrophys.* 558, A62. doi:10.1051/0004-6361/201321686

Keller, L. P., Hony, S., Bradley, J. P., Molster, F. J., Waters, L. B. F. M., Bouwman, J., et al. (2002). Identification of iron sulphide grains in protoplanetary disks. *Nature* 417, 148–150. doi:10.1038/417148a

Kemper, F., De Koter, A., Waters, L. B. F. M., Bouwman, J., and Tielens, A. G. G. M. (2002). Dust and the spectral energy distribution of the OH/IR star OH 127.8+0.0: evidence for circumstellar metallic iron. *Astron. Astrophys.* 384, 585–593. doi:10.1051/0004-6361:20020036

Khodakov, A. Y., Chu, W., and Fongarland, P. (2007). Advances in the development of novel cobalt Fischer-Tropsch catalysts for synthesis of long-chain hydrocarbons and clean fuels. *Chem. Rev.* 107, 1692–1744. doi:10.1021/cr050972v

Kress, M. E., and McKay, C. P. (2004). Formation of methane in comet impacts: implications for Earth, mars, and titan. *Icarus* 168, 475–483. doi:10.1016/j.icarus.2003.10.013

Kühne, T. D., Iannuzzi, M., Del Ben, M., Rybkin, V. V., Seewald, P., Stein, F., et al. (2020). CP2K: an electronic structure and molecular dynamics software package - Quickstep: efficient and accurate electronic structure calculations. *J. Chem. Phys.* 152, 194103. doi:10.1063/5.0007045

Kwok, S. (2004). The synthesis of organic and inorganic compounds in evolved stars. *Nature* 430, 985–991. doi:10.1038/nature02862

Lammer, H., Zerkle, A. L., Gebauer, S., Tosi, N., Noack, L., Scherf, M., et al. (2018). Origin and evolution of the atmospheres of early Venus, Earth and Mars. *Astron. Astrophys. Rev.* 26, 2–72. doi:10.1007/s00159-018-0108-y

Lee, C., Yang, W., and Parr, R. G. (1988). Development of the Colle-Salvetti correlation-energy formula into a functional of the electron density. *Phys. Rev. B* 37, 785–789. doi:10.1103/physrevb.37.785

Li, A., and Greenberg, J. M. (2002). Mid-infrared spectropolarimetric constraints on the core-mantle interstellar dust model. *Astrophys. J.* 577, 789–794. doi:10.1086/342222

Li, H. J., Chang, C. C., and Ho, J. J. (2011). Density functional calculations to study the mechanism of the Fischer-Tropsch reaction on Fe(111) and W(111) surfaces. *J. Phys. Chem. C* 115, 11045–11055. doi:10.1021/jp112372g

Lippert, G., Hutter, J., and Parrinello, M. (1997). A hybrid Gaussian and plane wave density functional scheme. *Mol. Phys.* 92, 477–487. doi:10.1080/00268979709482119

Llorca, J. (2002). Are organic molecules produced by nebular Fischer-Tropsch processes preserved in comets? *Adv. Sp. Res.* 30, 1469–1472. doi:10.1016/s0273-1177(02)00506-9

Llorca, J., and Casanova, I. (1998). Formation of carbides and hydrocarbons in chondritic interplanetary dust particles: a laboratory study. *Meteorit. Planet. Sci.* 33, 243–251. doi:10.1111/j.1945-5100.1998.tb01629.x

Lodders, K., and Amari, S. (2005). Presolar grains from meteorites: remnants from the early times of the solar system. *Chem. Erde* 65, 93–166. doi:10.1016/j.chemer.2005.01.001

Lodders, K., and Fegley, B. (1999). Condensation chemistry of circumstellar grains. *Symp. - Int. Astron. Union* 191, 279–290. doi:10.1017/s0074180900203185

Marcus, R. A. (1952). Unimolecular dissociations and free radical recombination reactions. *J. Chem. Phys.* 20, 359–364. doi:10.1063/1.1700424

Marini, E., and Tosi, S. (2025). Mass-loss and silicate production in oxygen-rich AGB stars: current understanding and open questions. *Front. Astron. Sp. Sci.* 12, 1581269. doi:10.3389/fspas.2025.1581269

Martinez-Bachs, B., Anguera-Gonzalez, A., Pareras, G., and Rimola, A. (2024). Formation of methanol via fischer-tropsch catalysis by cosmic iron sulphide. *ChemPhysChem* 25, e202400272. doi:10.1002/cphc.202400272

McCarthy, M. C., Gottlieb, C. A., and Cernicharo, J. (2019). Building blocks of dust: a coordinated laboratory and astronomical study of the archtype AGB carbon star IRC+10216. *J. Mol. Spectrosc.* 356, 7–20. doi:10.1016/j.jms.2018.11.018

Molpeceres, G., Zaverkin, V., Furuya, K., Aikawa, Y., and Kästner, J. (2023). Reaction dynamics on amorphous solid water surfaces using interatomic machine-learned potentials: microscopic energy partition revealed from the P + H → PH reaction. *Astron. Astrophys.* 673, A51. doi:10.1051/0004-6361/202346073

Öberg, K. I., Guzmán, V. V., Merchantz, C. J., Qi, C., Andrews, S. M., Cleeves, L. I., et al. (2017). H 2 CO distribution and formation in the TW HYA disk. *Astrophys. J.* 839, 43. doi:10.3847/1538-4357/aa689a

Pareras, G., Cabedo, V., McCoustra, M., and Rimola, A. (2023). Single-atom catalysis in space: computational exploration of Fischer- Tropsch reactions in astrophysical environments. *Astron. Astrophys.* 680, A57. doi:10.1051/0004-6361/202347877

Pareras, G., Cabedo, V., McCoustra, M., and Rimola, A. (2024). Single-atom catalysis in space-II. Ketene–acetaldehyde–ethanol and methane synthesis via Fischer-Tropsch chain growth. *Astron. Astrophys.* 687, A230. doi:10.1051/0004-6361/202449378

Perdew, J. P., Ruzsinszky, A., Csonka, G. I., Vydrov, O. A., Scuseria, G. E., Constantin, L. A., et al. (2008). Restoring the density-gradient expansion for exchange in solids and surfaces. *Phys. Rev. Lett.* 100, 136406. doi:10.1103/physrevlett.100.136406

Podio, L., Bacciotti, F., Fedele, D., Favre, C., Codella, C., Rygl, K. L. J., et al. (2019). Organic molecules in the protoplanetary disk of DG Tauri revealed by ALMA. *Astron. Astrophys.* 623, L6. doi:10.1051/0004-6361/201834475

Polanyi, M., and Wigner, E. (1928). Über die Interferenz von Eigenschwingungen als Ursache von Energieschwankungen und chemischer Umsetzungen. *Z. für Phys. Chem.* 139A, 439–452. doi:10.1515/zpch-1928-13930

Psaradaki, I., Costantini, E., Rogantini, D., Mehdipour, M., Corrales, L., Zeegers, S. T., et al. (2023). Oxygen and iron in interstellar dust: an X-ray investigation. *Astron. Astrophys.* 670, A30. doi:10.1051/0004-6361/202244110

Qi, C., Öberg, K. I., and Wilner, D. J. (2013). H2CO and N2H+ in protoplanetary disks: EVIDENCE for a CO-ice regulated chemistry. *Astrophys. J.* 765, 34. doi:10.1088/0004-637X/765/1/34

Reuter, D. C. (1992). The contribution of methanol to the 3.4 micron emission feature in comets. *Astrophys. J.* 386, 330. doi:10.1086/171019

Ridgway, S. T., Hall, D. N. B., Kleinmann, S. G., Weinberger, D. A., and Wojslaw, R. S. (1976). Circumstellar acetylene in the infrared spectrum of IRC +10° 216. *Nature* 264, 345–346. doi:10.1038/264345a0

Roy, A., Surendra, V. S., Ramachandran, R., Meka, J. K., Gupta, S., Janardhan, P., et al. (2023). Interstellar carbonaceous dust and its formation pathways: from an experimental astrochemistry perspective. *J. Indian Inst. Sci.* 103, 919–938. doi:10.1007/s41745-023-00393-6

Rubin, M., Altwegg, K., Balsiger, H., Berthelier, J. J., Combi, M. R., de Keyser, J., et al. (2019). Elemental and molecular abundances in comet 67P/Churyumov-Gerasimenko. *Mon. Not. R. Astron. Soc.* 489, 594–607. doi:10.1093/mnras/stz2086

Saikia, G., Gogoi, R., Gupta, R., and Vaidya, D. B. (2019). Modelling the mid-infrared polarization in dust around young stars. *Mon. Not. R. Astron. Soc.* 484, 3582–3589. doi:10.1093/mnras/stz231

Sargent, B. A., Forrest, W. J., Tayrien, C., McClure, M. K., Watson, D. M., Sloan, G. C., et al. (2009). Dust processing and grain growth in protoplanetary disks in the taurus-auriga star-forming region. *Astrophys. J. Suppl. Ser.* 182, 477–508. doi:10.1088/0067-0049/182/2/477

Sasaki, S., Nakamura, K., Hamabe, Y., Kurahashi, E., and Hiroi, T. (2001). Production of iron nanoparticles by laser irradiation in a simulation of lunar-like space weathering. *Nature* 410, 555–557. doi:10.1038/35069013

Sekine, Y., Sugita, S., Shido, T., Yamamoto, T., Iwasawa, Y., Kadono, T., et al. (2006). An experimental study on fischer-tropsch catalysis: implications for impact phenomena and nebular chemistry. *Meteorit. Planet. Sci.* 41, 715–729. doi:10.1111/j.1945-5100.2006.tb00987.x

Speck, A. K., Hofmeister, A. M., and Barlow, M. J. (1999). The S[CLC]i[/CLC]C problem: astronomical and meteoritic evidence. *Astrophys. J.* 513, L87–L90. doi:10.1086/311891

Speck, A. K., Thompson, G. D., and Hofmeister, A. M. (2005). The effect of stellar evolution on SiC dust grain sizes. *Astrophys. J.* 634, 426–435. doi:10.1086/496955

Stökl, A., Dorfi, E. A., Johnstone, C. P., and Lammer, H. (2016). Dynamical accretion of primordial atmospheres around planets with masses between 0.1 and 5 M⊕ in the habitable zone. *Astrophys. J.* 825, 86. doi:10.3847/0004-637x/825/2/86

Sun, W. Z., Jin, G. Q., and Guo, X. Y. (2005). Partial oxidation of methane to syngas over Ni/SiC catalysts. *Catal. Commun.* 6, 135–139. doi:10.1016/j.catcom.2004.11.013

Tian, M., Liu, B. S., Hammonds, M., Wang, N., Sarre, P. J., and Cheung, A. S. C. (2012). Formation of polycyclic aromatic hydrocarbons from acetylene over nanosized olivine-type silicates. *Phys. Chem. Chem. Phys.* 14, 6603–6610. doi:10.1039/c2cp23309f

Tian, M., Liu, B. S., Hammonds, M., Wang, N., Sarre, P. J., and Cheung, A. S. C. (2013). Catalytic conversion of acetylene to polycyclic aromatic hydrocarbons over particles of pyroxene and alumina. *Philos. Trans. R. Soc. A Math. Phys. Eng. Sci.* 371, 20110590. doi:10.1098/rsta.2011.0590

Tielens, A. G. G. M. (2008). Interstellar polycyclic aromatic hydrocarbon molecules. *Annu. Rev. Astron. Astrophys.* 46, 289–337. doi:10.1146/annurev.astro.46.060407.145211

Van Der Laan, G. P., and Beenackers, A. A. C. M. (1999). Kinetics and selectivity of the fischer-tropsch synthesis: a literature review. *Catal. Rev. - Sci. Eng.* 41, 255–318. doi:10.1081/cr-100101170

Vandevondele, J., Krack, M., Mohamed, F., Parrinello, M., Chassaing, T., and Hutter, J. (2005). Quickstep: fast and accurate density functional calculations using a mixed Gaussian and plane waves approach. *Comput. Phys. Commun.* 167, 103–128. doi:10.1016/j.cpc.2004.12.014

Vannice, M. A., Chao, Y. L., and Friedman, R. M. (1986). The preparation and use of high surface area silicon carbide catalyst supports. *Appl. Catal.* 20, 91–107. doi:10.1016/s0166-9834(00)83172-3

Varga, J., Waters, L. B. F. M., Hogerheijde, M., Van Boekel, R., Matter, A., Lopez, B., et al. (2024). Mid-infrared evidence for iron-rich dust in the multi-ringed inner disk of HD 144432. *Astron. Astrophys.* 681, A47. doi:10.1051/0004-6361/202347535

Walsh, C., Loomis, R. A., Öberg, K. I., Kama, M., van 't Hoff, M. L. R., Millar, T. J., et al. (2016). First detection of gas-phase methanol in a protoplanetary disk. *Astrophys. J.* 823, L10. doi:10.3847/2041-8205/823/1/l10

Walsh, C., Vissapragada, S., and McGee, H. (2017). Methanol formation in TW Hya and future prospects for detecting larger complex molecules in disks with ALMA. *Proc. Int. Astron. Union* 13, 395–402. doi:10.1017/s1743921317007037

Whittet, D. C. B., Duley, W. W., and P, G. M. (1990). On the abundance of silicon carbide dust in the interstellar medium. *Mon. Not. R. Astron. Soc.* 244, 427–431.

Woitke, P. (2006). Too little radiation pressure on dust in the winds of oxygen-rich AGB stars. *Astron. Astrophys.* 460, L9–L12. doi:10.1051/0004-6361:20066322

Woods, P. M., Millar, T. J., Zijlstra, A. A., and Herbst, E. (2002). The synthesis of benzene in the proto–planetary nebula CRL 618. *Astrophys. J.* 574, L167–L170. doi:10.1086/342503

Wu, P., Wang, J., Li, Y., He, C., Xie, Z., and Duan, C. (2011). Luminescent sensing and catalytic performances of a multifunctional lanthanide-organic framework comprising a triphenylamine moiety. *Adv. Funct. Mater.* 21, 2788–2794. doi:10.1002/adfm.201100115

Zarkevich, N. A., and Johnson, D. D. (2015). Nudged-elastic band method with two climbing images: finding transition states in complex energy landscapes. *J. Chem. Phys.* 142, 024106. doi:10.1063/1.4905209

Zhang, H. B., You, X., and Law, C. K. (2015). Role of spin-triplet polycyclic aromatic hydrocarbons in soot surface growth. *J. Phys. Chem. Lett.* 6, 477–481. doi:10.1021/jz502635t

Zhao, T. Q., Li, Q., Liu, B. S., Gover, R. K. E., Sarre, P. J., and Cheung, A. S. C. (2016). Laboratory astrochemistry: catalytic conversion of acetylene to polycyclic aromatic hydrocarbons over SiC grains. *Phys. Chem. Chem. Phys.* 18, 3489–3496. doi:10.1039/c5cp06425b

Ziurys, L. M. (2024). Prebiotic astrochemistry from astronomical observations and laboratory spectroscopy. *Annu. Rev. Phys. Chem.* 75, 307–327. doi:10.1146/annurev-physchem-090722-010849